ELSEVIER

Materials Science and Engineering A365 (2004) 46–56

MATERIALS SCIENCE & ENGINEERING A

www.elsevier.com/locate/msea

Multiscale modelling of radiation damage in metals: from defect generation to material properties

D.J. Bacon*, Yu.N. Osetsky

Materials Science and Engineering, Department of Engineering, The University of Liverpool, Brownlow Hill, Liverpool L69 3GH, UK

Abstract

Atomic- and continuum-scale computer simulation techniques have now become sufficiently powerful that many phenomena associated with radiation damage effects in metals can be modelled with a high degree of realism. Recent studies of several such phenomena are reviewed here. Primary knock-on atoms (PKAs) that recoil under collision from energetic atomic particles such as neutrons or ions are the principal source of damage. At high enough recoil energy, they create cascades of atomic displacements that result in single and clustered self-interstitial and vacancy defects. The time and length scales of the cascade process are ideally suited to atomic-scale computer simulation by molecular dynamics (MD). This method provides data on the number of defects produced and their distribution in clusters. This information was not available from earlier models and so the nature of the primary damage state is now much clearer. MD is also being used to reveal the nature of the motion and interaction of defects. Prediction and understanding of mechanical properties of irradiated metals requires simulation of dislocation–obstacle interactions. Models based on the continuum approximation are now being extended by large-scale MD simulations of the motion of dislocations gliding through irradiation-induced features such as voids and precipitates, and these reveal the strength and weakness of the earlier studies. Dynamic effects at temperatures greater than 0 K are also being investigated. The place of modelling in the multiscale problems of radiation damage is emphasised.

Keywords: Computer simulation; Multiscale modelling; Radiation damage; Displacement cascades; Defect clusters; Dislocation–obstacle interactions

1. Introduction

The role of multiscale computer modelling has become firmly established in recent years for several reasons. First, computer power has grown enormously. Second, this power and the development of techniques and underlying theory mean that many of the properties of materials can now be simulated by computer with a high level of realism. Third, simulation enables some phenomena that are not amenable to experimental study to be investigated.

Core materials of nuclear power installations operate at high temperature and suffer high fluxes of fast neutrons from the fission reaction, and the result can be a significant change in microstructure and a degradation of properties. The phenomena involved include processes over wide ranges of length and time scales, i.e. from defect production at the atomic-level ($\sim 10^{-15}$ s, 10^{-10} m) to microstructure evolution that can take years to achieve ($\sim 10^{9}$ s, 10^{-3} m). Ideally, progress in understanding and predicting material properties requires modelling across these scales, and atomic-scale computer simulation, the main topic of this article, provides a route from electronic/atomic processes to phenomena at the continuum-level. It can be used to obtain quantitative input to models used for the higher levels, such as Monte Carlo and rate theory studies of microstructure evolution, and continuum models of dislocation dynamics in metals under applied stress.

In the present paper, we review some recent work on the creation of the primary form of radiation damage in displacement cascade in metals, the properties of the defects produced and the effect of the products of damage on dislocation motion under applied stress.

2. The scale and nature of cascade damage

Displacement cascades are the primary source of radiation damage during fast-neutron and heavy-ion irradiation of metals and are generated by the recoil of primary knock-on

* Corresponding author. Tel.: +44-151-794-4662; fax: +44-151-794-4675.
E-mail address: djbacon@liv.ac.uk (D.J. Bacon).

0921-5093/$ – see front matter © 2003 Elsevier B.V. All rights reserved.
doi:10.1016/j.msea.2003.09.006

atoms (PKAs) that result from elastic collisions of the neutrons or ions with atoms from the host lattice. Recoil energy spectra can range up to tens of kiloelectronvolt in components in nuclear plant. The primary and secondary collisions cause the temporary displacement of many (typically thousands) of atoms and the failure of some to return to lattice sites following this collision phase gives rise to a localised, high supersaturation of point defects, with vacancies near the centre of the cascade zone and self-interstitial atoms (SIAs) towards the outside. The displacement of atoms to new sites can also change the local chemistry in alloys. Subsequent evolution of these defects give rises to important changes that affect the performance of metals, and understanding these is crucial for assessing material suitability for service.

The cascade process is characterised by lengths and times of the order of nanometre and picoseconds, respectively, and is not open to direct experimental study. These scales are ideally suited to atomic-scale computer simulation using molecular dynamics (MD), however, and the details of the cascade process have become clear from MD simulations [1–3]. Typical MD simulation of displacement cascades involves models of crystals containing up to few million atoms, which interact via relatively simple empirical many-body potentials (MBP). One atom is chosen as the PKA by being given a kinetic energy, E_p, and the simulation is usually continued until the temperature of the cascade region decreases to the ambient. The output can include the total number and coordinates of the surviving vacancy or interstitial defects at the end of cooling phase, the fraction of each formed in clusters, the size distribution and structure of these clusters, and atomic displacements (for characterisation of mixing). Ideally, a few tens of events at each condition of PKA energy and crystal temperature should be simulated to achieve statistically representative results [4,5].

Extensive information has been obtained during the last decade on the nature of primary damage in cascades in the bulk of pure bcc, fcc and hcp metals, some binary and ordered alloys, and near metal surfaces, e.g. [1,4–18], respectively, and the basic processes have been clarified. One of the most significant is that extensive recombination of SIAs and vacancies occurs during the cooling phase of the thermal spike in the cascade zone. As a consequence, the total number, N_F, of point defects (vacancy or SIA) surviving at the end of the cascade process is significantly lower than the number, N_{NRT}, predicted by the NRT model [19] for a given cascade energy E_p. Data for Cu simulated at 100 K using two different interatomic potentials [5] and high statistics of treated cascades (from 25 to 40 cascades for each energy) is presented in Fig. 1. The data for N_F obtained from numerous simulation studies show that the defect production efficiency, N_F/N_{NRT}, follows the same trend for all metals as that in Fig. 1, and saturates in the region of 0.1–0.3 above about 5 keV. Compilations [1–4] show that the dependence of N_F on E_p fits the relationship $N_F = A\,(E_p)^m$ first found

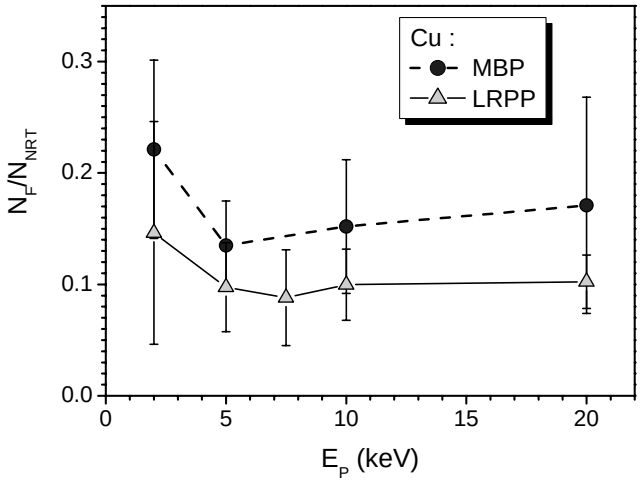

Fig. 1. Number, N_F, of vacancy–SIA pairs surviving at the end of the cooling stage of displacement cascades of energy E_p in Cu, normalised by the NRT-predicted number, N_{NRT}. The simulations used many-body (MBP) and long-range pair potentials (LRPP) [5]. Symbols indicate the mean and bars the standard error.

in [20] very well for cascade energy up to ~20–30 keV. The exponent m is typically ~0.7–0.8, unlike the value 1 in the NRT formula, and m and A are only weakly dependent on material and ambient temperature. There is no discernible dependence on crystal structure, and so differences between the damage microstructure in pure bcc, fcc and hcp metals observed in experiment (e.g. [21–23]) are not due to differences in defect production efficiency in the cascade process itself. The MD data are consistent with experiments (e.g. [24–26]) that show the production efficiency of defects visible by TEM in pure metals and alloys under cascade-producing ion and neutron-irradiation is approximately one quarter of the NRT value. As the PKA energy increases, there is an increased tendency for cascades to break up into distinct sub-cascades, resulting in a slight increase in m [27,28]. This transition occurs at lower energy in the lighter metals.

With regard to cascade damage in alloys, there is no evidence from MD studies so far that alloying elements in solution or in ordered phases have a significant effect on the number of vacancies and SIAs created in the primary state of cascades. However, the atomic displacements in cascades create additional effects in ordered alloys, either because disorder is created when sites in the individual sub-lattices become occupied by atoms of the wrong type, i.e. anti-site defects, or crystalline order is not restored and an amorphous structure is formed. Computer simulation has been used to investigate both aspects, e.g. [29–33], and shows that the damage zone corresponds largely to the 'molten' core region formed in the thermal spike, and that the number of anti-site defects per cascade increases with increasing E_p as in the power law equation above, but with an exponent of ~1.25 rather than approximately 0.75 as found for N_F.

3. The formation and properties of defect clusters

Apart from providing information on the number of point defects, MD modelling has also revealed details of the clustering of these defects that occurs in the cascade process. The collapse of the lattice around vacancy clusters (VC) in the core of cascades into dislocation loops (DLs) or stacking fault tetrahedra (SFTs) has been observed in many metals as a result of heavy-ion irradiation of thin foils [34] and these extended defects are also found in neutron-irradiated metals [35]. However, the probability with which such defects form and their efficiency for retaining the vacancies are strongly dependent on the crystal structure and atomic mass. Simulation results are consistent with this. Thus, large compact clusters have been found only simulations of fcc and hcp metals. In Cu (fcc), they are perfect or truncated SFTs, e.g. [4,5,36], while in α-Zr (hcp) they are planar defects similar to prism or basal dislocation loops, e.g. [12,37]. An example of the debris created in the simulation of a 25 keV cascade in Cu at 100 K is shown in Fig. 2. The collapsed vacancy cluster is seen to be two conjoined, truncated SFTs. Most MD modelling of bcc metals has been on α-Fe and no large compact planar or three-dimensional (3-D) vacancy clusters have been created. This is consistent with experiments on this metal [34], for which cascade collapse has only been observed following irradiation by heavy ions that produce cascades with high energy density. Instead, simulations reveal loose complexes of vacancies in second and higher-order neighbour shells [7,8,38,39]. The most extensive statistics on vacancy clustering (each defect having at least one nearest neighbour) have been obtained for Cu [4,5] where a PKA of 10–20 keV energy produces one cluster of about five vacancies on average, and ∼25% of the surviving vacancies are in clusters. Data on the dependence of intracascade vacancy clustering on energy and temperature in Cu is presented in Fig. 3. The fraction of vacancies in clusters of size three or more is seen to be insensitive to temperature.

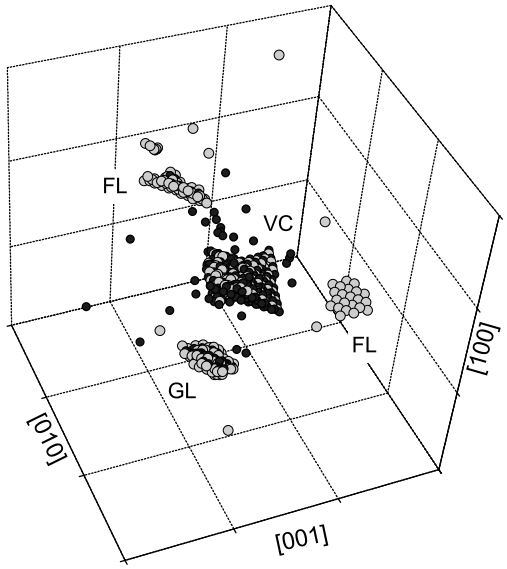

Fig. 2. Computer-generated image showing the vacant sites (dark spheres) and atoms in interstitial sites (light spheres) created in a 25 keV cascade in a model of copper at 100 K [2]. The grid size is $10a_0$, where a_0 is the lattice parameter. The actual MD model contained 2,048,000 atoms, most of which are not shown. The final defect state of 115 vacancies and SIAs is dominated by perfect glissile (GL) and faulted sessile (FL) interstitial dislocation loops and a vacancy cluster (VC) consisting of two conjoined stacking fault tetrahedra.

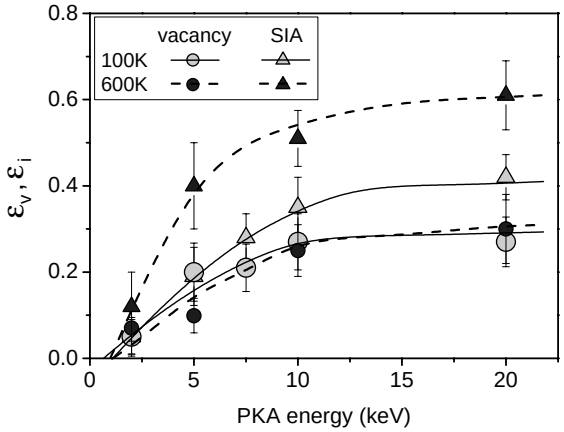

Fig. 3. The fractions of vacancies (ε_v) and interstitials (ε_i) surviving in clusters containing ≥3 point defects vs. PKA energy, E_p, in Cu at either 100 or 600 K [5].

The formation of SIA clusters within the cascade process itself was found in early MD modelling of Cu [40] and predicted in diffusion-based theoretical calculations [41]. The formation of small clusters is consistent with previous experimental measurement of diffuse X-ray scattering in neutron-irradiated metals, e.g. [42]. It is now known from MD that SIA clusters can form with a size distribution comparable to the vacancy component, and SIA loops visible by TEM have been reported recently [43]. Intracascade clustering has been a common feature of all reported MD simulations of cascades in metals, irrespective of the crystal structure. In Cu, for example, each cascade with E_p in the range 10–20 keV yields one to two SIA clusters of mean size ∼5–6 defects [5]. The fraction of SIAs in clusters, ε_i, lies in the range of 50–60%. Data for the energy and temperature dependence of the fraction of SIAs in clusters of size three or more in Cu is presented in Fig. 3. It is seen that unlike the clustered vacancy fraction, the number of SIA defects per cluster increases at high temperature, although the number of clusters per cascade decreases. These effects are believed to result from enhanced SIA motion in the longer thermal spike and a tendency for cascades to have higher energy and defect density at the end of the collision phase at high temperature. The high value of the fraction, of the interstitial population produced in clusters in the cascade process itself is important because interstitial clusters are thermally stable and, if they can move away from their parent cascade (see below), can be absorbed preferentially at sinks such as dislocations

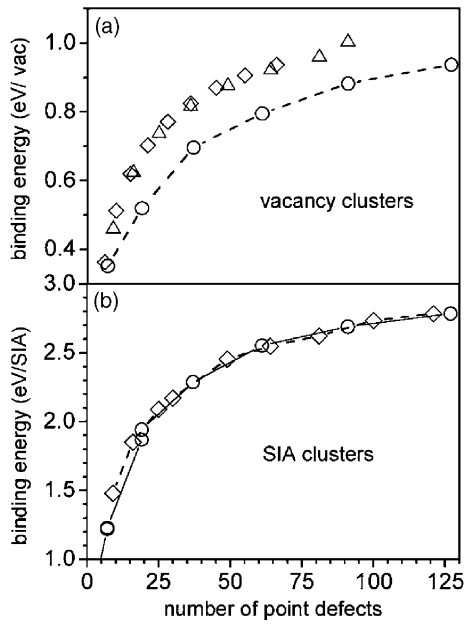

Fig. 4. Binding energy of SIA and vacancy clusters in Cu [46,47]. Circles: faulted 1/3⟨1 1 1⟩ Frank loops; diamonds: rhombus-shaped 1/2⟨1 1 0⟩ perfect loops; triangles: SFTs.

and boundaries. Vacancy clusters, however, are not stable and dissociate into single vacancies at high enough temperature, leading to a 'production bias' in favour of vacancies in the supply of point defects from cascades [44]. The relative stability of clusters of different nature is illustrated in Fig. 4, where binding energy data obtained by atomic-scale simulation for various vacancy and SIA clusters in Cu is plotted.

The majority of SIA clusters have the form of perfect (and therefore glissile) dislocation loops. The SIA platelet labelled GL in Fig. 2 is an example of a loop with Burgers vector $\boldsymbol{b} = 1/2\langle 1\,1\,0\rangle$ in Cu. Clusters having a sessile configuration have also been observed in MD simulations, to an extent that is metal-dependent. The fraction is lowest (a few percent) in bcc metals, where such clusters take the form of metastable three-dimensional arrangements of SIAs [45], and highest (up to ∼30–40%) in low stacking fault energy fcc metals, where faulted Frank dislocation loops with $\boldsymbol{b} = 1/3\langle 1\,1\,1\rangle$ commonly arise [4,5]. The defects labelled FL in Fig. 2 are examples of the latter. The sessile fraction in hcp metals lies between these extremes.

The use of the word 'glissile' in the preceding paragraph is important because it implies that such defects are mobile by the process of dislocation glide. In fact, perfect dislocation loops, whether vacancy or interstitial in nature, are intrinsically mobile. However, the mobility of glissile SIA clusters has gained more attention because of their more common occurrence and stability. Strictly, a small cluster (up to a few tens of SIAs) discussed here is the nucleus of a dislocation loop because it has the morphology and distortion field of compact planar set of crowdions, rather than a Volterra dislocation. The crowdion axis is the direction of the Burgers vector: $1/2\langle 1\,1\,0\rangle$ in fcc, $1/2\langle 1\,1\,1\rangle$ or $\langle 1\,0\,0\rangle$ in bcc and $1/3\langle 1\,1\,\bar{2}\,0\rangle$ in hcp [48–51]. These small perfect 'dislocation loops' perform fast thermally-activated 1-D motion and only small clusters (<3 or 4 SIAs) change their glide direction $\boldsymbol{b}$ during the period of MD simulation, which is typically ∼10 ns. Mobility decreases with increasing size, but the activation energy does not depend on size and is close to that of an individual crowdion of the corresponding type, i.e. ∼0.02 eV [48–52]. However, the thermally-activated motion of loops is suppressed at large size, e.g. above ∼300 SIAs for $1/2\langle 1\,1\,1\rangle$ clusters in Fe and ∼120 SIAs for $1/2\langle 1\,1\,0\rangle$ clusters in Cu [16,50]. In the latter case, this is because of the formation of sessile stair-rod partials at the loop corners after the sides have dissociated on the ⟨1 1 1⟩ glide prism. Another crystallographic effect arises in the hcp structure. The $\langle 1\,1\,\bar{2}\,0\rangle$ directions lie only in the basal plane, and so transport of matter by the glide of SIA clusters is two-dimensional. In the bcc and fcc metals, however, the glide directions are distributed in three-dimensions and so although individual loops move in one-dimension only, the associated material transport is three-dimensional.

The thermally-activated 1-D motion of clusters should not be described as a conventional diffusion process, but attempts have been made to parameterise it as correlated 1-D diffusion. The jump frequency of the cluster centre of mass, correlation factor and effective migration energy have been estimated for clusters containing up to 91 SIAs in Fe, Cu and Zr [50,51,53] and qualitatively similar results were obtained in all cases. Some data for ⟨1 1 1⟩ crowdion clusters in Fe are presented in Fig. 5 (as noted above, vacancy clusters that collapse to form loops with a perfect $\boldsymbol{b}$ are also glissile and a recent MD study has shown that their mobility in α-Fe is only slightly lower than that of clusters of the same number of interstitials [16]). Clusters of ⟨1 0 0⟩ crowdions behave in a similar fashion [50], but with slightly higher activation energy. It has been shown that the mechanism of

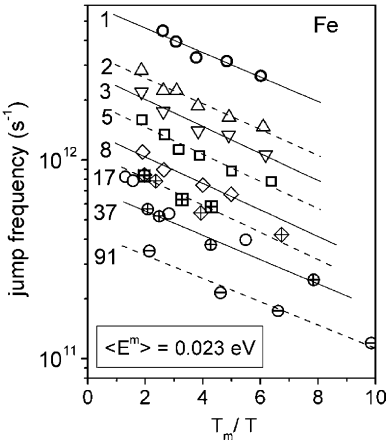

Fig. 5. Jump frequency of the centre of mass of SIA clusters consisting of ⟨1 1 1⟩ crowdions in α-Fe at different temperatures (T) [50]. The number at the left of each data line is the number of interstitials in the cluster and T_m is the melting temperature in K.

cluster motion can be described as near-stochastic jumps of crowdions, with the probability to move the cluster centre of mass being inversely proportional to the number of SIAs in the cluster [53]. The effective correlation factor is significantly larger than unity, and clusters can move preferentially in one direction over large distance before a reversal, e.g. up to tens of nanometres over tens of picoseconds. This effect increases at low temperature and may be due to the influence of particular phonons, but, as yet, the physical basis for this fast thermally-activated glide is not fully understood. Nevertheless, the parameters obtained can be used in higher level modelling of microstructure evolution and damage accumulation [54].

4. Interactions involving SIA clusters

The high stability and mobility of glissile SIA crowdion clusters, and the long-range strain field they create along their glide path, affect their interactions with each other and other defects in a metal, and are thus important factors to be taken into account in multiscale models developed to predict microstructure evolution during irradiation under cascade damage conditions. Several types of interaction have been studied to date.

The interaction between clusters and point defects or other clusters can lead to growth, shrinkage or annihilation, and can also result in changes in cluster character, e.g. glissile ⇔ sessile transformation. Interactions of this type are common in cascades, where their probability is increased by the high local concentration of defects, and have been observed in simulations of cascades in Fe [45] and Cu [4,5,11]. The probability of observing sessile SIA clusters is much higher in Cu than in Fe due to existence of the stable stacking fault on $\{1\,1\,1\}$ planes. They may form during the thermal spike phase or by subsequent mutual interaction of clusters. An example of the latter process in which three crowdion clusters interact to create a faulted platelet lying on a $\{1\,1\,1\}$ plane in Cu is presented in Fig. 6.

In some interactions, the mobility of glissile SIA clusters may be reduced or cease without change of structure. Examples observed in MD simulations include a $1/2\langle 1\,1\,1\rangle$ cluster in Fe interacting with a vacancy [47] or an interstitial impurity atom [55]. The effect is particularly strong for C in Fe, where the solute atom becomes trapped at the cluster edge, and although it can move around the cluster by core diffusion, the cluster itself is prevented from gliding (at 300 K). It is possible that, at high enough temperature, the solute could be dragged by the cluster one-dimensionally towards the latter's own sink in the microstructure.

SIA cluster growth and shrinkage by point defect interaction has been found to be material-dependent. In bcc Fe, a vacancy can be absorbed at the cluster edge and thus reduce the cluster size [47]. The process is more complicated in Cu and depends on cluster size [56]. A vacancy can recombine with an interstitial in the edge of small clusters or simply

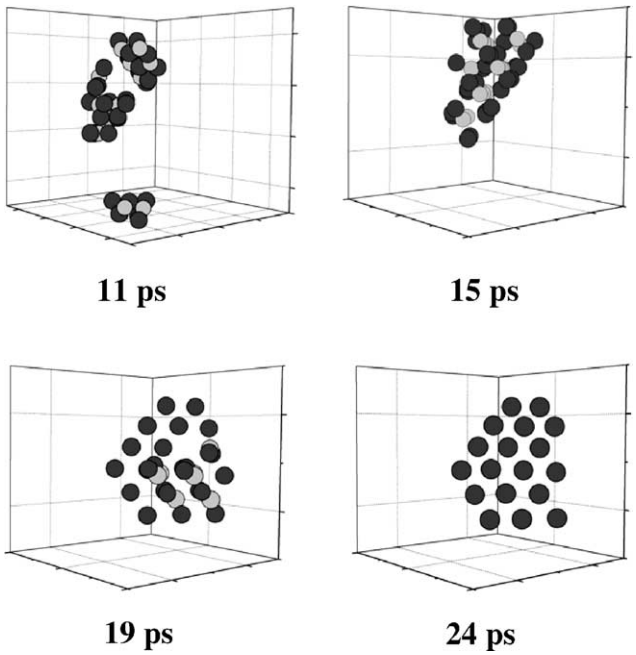

Fig. 6. Three $1/2\langle 1\,1\,0\rangle$ glissile SIA clusters coalesce to form the nucleus of a sessile $1/3\langle 1\,1\,1\rangle$ Frank loop during simulation of a 20 keV cascade in Cu [4]. The time after the PKA creation is indicated for each configuration. Dark spheres are interstitial atoms, light spheres are vacant sites. The projection direction is close to $\langle 1\,1\,1\rangle$.

reduce cluster mobility if it lies inside the glide prism, as in Fe. However, larger clusters do not easily absorb a vacancy because of dissociation of the bounding dislocation on the glide prism and their glide is simply prevented. The situation in hcp Zr falls between these two extremes [56], for a vacancy can be annihilated on a $\{1\,0\,\bar{1}\,0\}$ face of an SIA cluster, where dissociation is weak, but behaves as in Cu on a $(0\,0\,0\,1)$ face, where dissociation occurs. Such peculiarities in cluster–vacancy interaction may lead to a difference in evolution of SIA clusters, in that growth may be partly suppressed in bcc metals.

Interaction between glissile clusters with parallel Burgers vector can lead to the formation of extended complexes of loops. Modelling by statics and MD in [57,58] has revealed that $1/2\langle 1\,1\,1\rangle$ SIA clusters which do not have overlapping glide prisms in Fe, attract each other and form a stable complex. The glissile nature of the clusters does not change, but the mobility of the complex depends on the number and size of the clusters within it: the complex retains mobility if the number of clusters is small (<5) and the total number of SIAs is about <300, but becomes immobile for larger numbers. A complex can grow further, attracting more glissile clusters with the same $\boldsymbol{b}$, thereby creating a raft of clusters/dislocation loops. However, this type of interaction between clusters with parallel glide cylinders can depend on the crystal structure, for in Cu glissile SIA clusters with $\boldsymbol{b} = 1/2\langle 1\,1\,0\rangle$ repel each other at large separation but attract at short distance, thereby creating an immobile complex, even for two small clusters. The reasons underlying

such behaviour are not yet understood. Nevertheless, the effects found in modelling are qualitatively consistent with experiment, for rafts of dislocation loops are observed in bcc but not fcc metals, e.g. [59,60].

Another interaction of considerable importance is that between clusters and dislocation lines. Although dislocations are generally sinks for mobile point defects, their ability to absorb glissile clusters depends on cluster nature and geometry, and the orientation of the Burgers vectors involved. In some circumstances, clusters create immobile jogs on the line and in others they can stand off from the line and form a decorating atmosphere. Furthermore, a dislocation gliding under stress can encounter clusters in or near the slip plane, and this can result in a resistance to its motion that depends on cluster properties and the Burgers vectors. In both situations, the yield and flow stress of the metal are changed by the products of radiation damage, and we discuss some recent modelling in this field in the following section.

5. Damage effects on dislocation behaviour

Recent research using atomic-level modelling to study the mechanisms involved in interactions between gliding dislocations and irradiation-induced obstacles has been made possible by large computing power. The models apply periodicity along the dislocation line direction, but the boundary conditions in the other two directions are chosen to suit the problem in hand. For example, the boundary regions may be fixed, with atoms displaced according to elasticity theory, or flexible, with atoms able to respond to unbalanced forces using either lattice or elastic Green functions, or partly periodic, so that the dislocation is one of an infinite row but is free to move over large distance (only edge dislocations have been treated with the third of these conditions). Both static and dynamic approaches are employed, but the latter is severely restricted when fixed or flexible boundary regions are used. The pros and cons of these methods, particularly with regard to research into dislocation dynamics, are discussed in a recent paper [61]. Current computer power allows systems of realistic size to be simulated, e.g. spacing between dislocations and between obstacles of about 100 nm in crystals of up to about 10 million atoms, with simulated times of over a few hundred picoseconds in dynamics modelling.

Molecular statics simulation has been used to study interactions between edge dislocations and defect clusters (voids, SFTs, SIA clusters) in bcc and fcc metals, e.g. [11,61,62]. An advantage of static simulation is that the results can be compared with line tension and self-stress treatments of dislocation–obstacle interaction based on elasticity theory, and can thus be used to estimate the flow stress. Also, they enable parameters required for continuum-level methods to be obtained, such as those used to simulate dislocation response to stress in continuum dislocation dynamics modelling.

The interaction between a moving edge dislocation and small glissile clusters of 4–37 SIAs was studied in Ni using MD by Rodney and Martin [63,64]. A variety of different dislocation-cluster geometries was considered and mechanisms involving cluster drag, absorption and annihilation at the dislocation line, and dislocation pinning and unpinning were observed. The drag of an SIA cluster by a moving edge dislocation has also been observed in α-Fe [11]. In this context, the high mobility of glissile clusters (Section 4) is important because it allows them to be attracted to the tensile side of edge dislocations [59,65]. Furthermore, loops having the same $\boldsymbol{b}$ as the dislocation can form a decoration, as noted in the preceding section. If immobile, such loops would raise the applied stress at which the line can glide away [65], but the MD simulations indicate they move with the dislocation. However, although decoration may not pin a dislocation directly, it is expected to increase the effective cross-section of interaction with obstacles in the microstructure and thereby increase the flow stress. This particular aspect is awaiting further study.

As observed in Section 3, SFTs are a common product of the vacancy component of cascade damage in fcc metals. The outcome of the interaction of dislocations with such defects is difficult to predict without atomic-scale modelling and some preliminary simulation studies of this process for a dissociated $1/2\langle 1\,1\,0\rangle$ edge dislocation and an SFT in Cu at zero (statics) and non-zero (dynamics) temperature have been reported [3,66]. It was found that an SFT can act as a rather strong obstacle to dislocation glide, in general, although the detailed mechanisms are not yet clear. The static simulations in [3] revealed that the vacancies in a regular SFT were rearranged as a dislocation passed through, as illustrated in Fig. 7, whereas the MD modelling in [66] indicated that the SFT can be absorbed by the dislocation. The resulting superjog reduced dislocation mobility. The ability of gliding dislocations to absorb the point defects in clusters formed in radiation damage is an important issue in understanding mechanical instability associated with yield point phenomena in irradiated metals. Diaz de la Rubia et al. [66] have shown by continuum-scale dislocation dynamics modelling that the slip channels observed in TEM to be clear of damage in such cases can be created when suitable defect absorption can occur.

In addition to dislocation loops and SFTs, voids and precipitates can also occur in the high supersaturation and fluxes of defects in irradiated metals. Their effect on the yield stress can be estimated to a first approximation using well-established elasticity theory treatments that were developed for unirradiated metals. However, the size of such defects and the possibility that they may be either absorbed or transformed by gliding dislocations limits the applicability of such an approach. Atomic-scale modelling is required and early results are now appearing.

Consider first voids. They attract dislocations by reducing the line length and so tend to pin them against further motion. At the simplest level, a void is a soft spot with

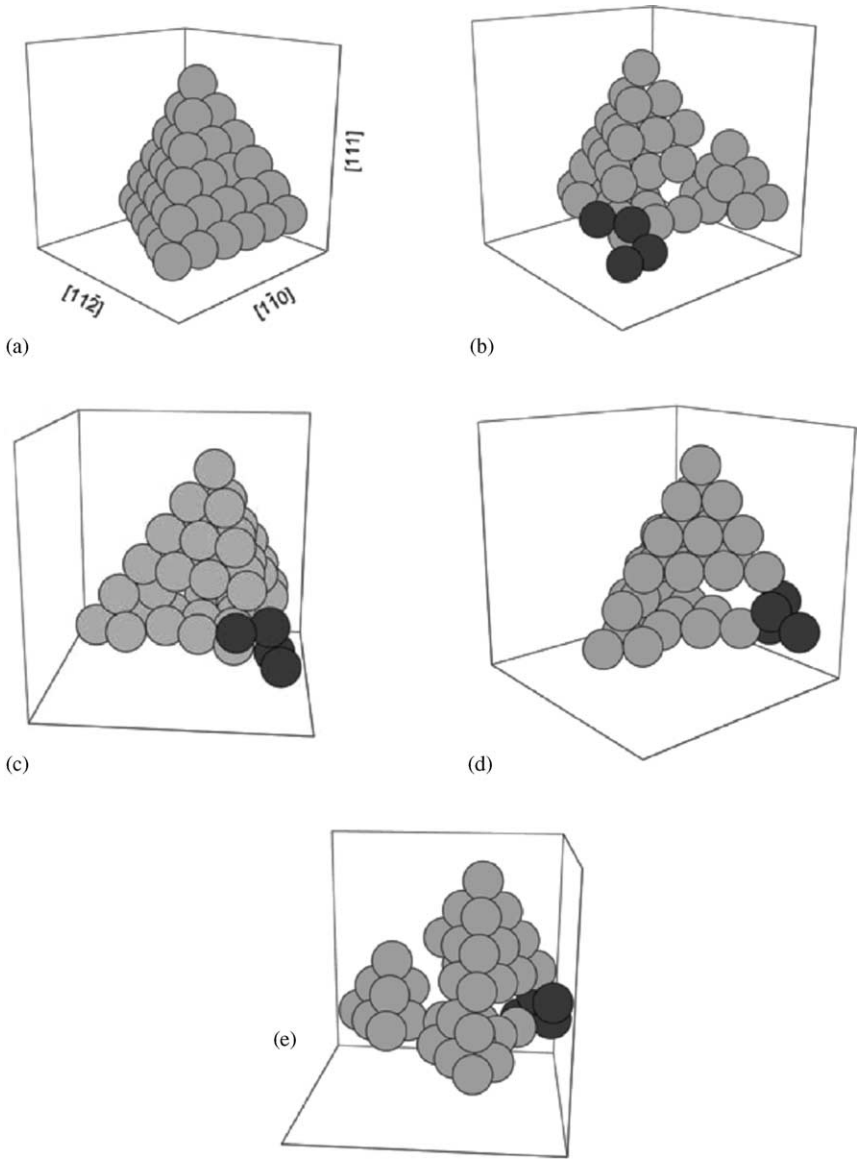

Fig. 7. Configuration of a 21-vacancy SFT in Cu at 0 K (a) before and (b) after interaction with a $1/2\langle 1\,1\,0\rangle$ dislocation. (c)–(e) are views after 45° rotations around the vertical axis. Light spheres indicate the position of atoms inside the SFT and dark spheres are atoms in fcc crystal lattice sites that experience high pressure [3].

zero elastic modulus, and the strengthening effect can be estimated by the Russell–Brown modulus hardening model [67]. This assumes constant line tension, neglects dislocation self-stress, i.e. the stress on one part of the line due to the others, and does not treat the boundary conditions where the line enters a void appropriately. A more rigorous method was employed by Scattergood and Bacon [68], who computed the self-stress of a flexible dislocation line constructed from piecewise segments using either isotropic or anisotropic elasticity theory. The dislocation boundary condition at the void surface was treated as follows. As a dislocation cuts through a void, it creates a surface step of length b (resolved along the direction of $\boldsymbol{b}$), and this is expected to restrict the cutting process. In the extreme, where the surface energy, γ_s, of the void is zero, Scattergood and Bacon used the approximation that the angle at which the line emerges from a void surface is the same as that for equilibrium of a straight dislocation impinging on a flat surface [69]. The effect of non-zero γ_s, which is the more realistic situation, was allowed for by modelling the angle of emergence as though a point force tangential to the void surface and proportional to γ_s and step size acts on the line where it intercepts the surface.

The equilibrium configurations of a dislocation forced to glide through of a row of voids of diameter D and spacing L under incrementally increasing resolved shear stress were obtained. The critical configuration at which the line overcomes the voids is that corresponding to the maximum

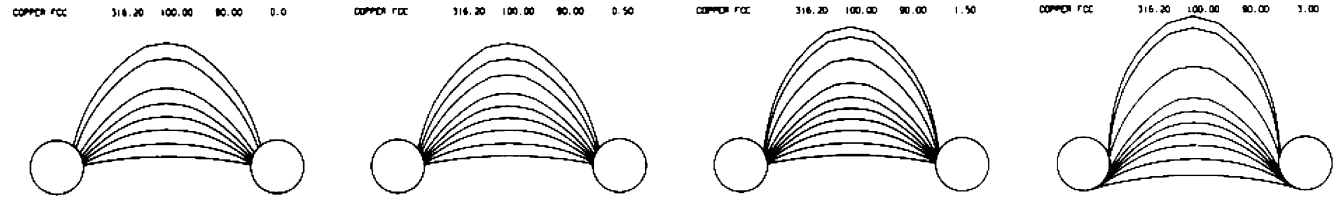

Fig. 8. Equilibrium line shapes obtained for a void row with $L = 316r_0$ and $D = 100r_0$ in Cu. Burgers vector $\boldsymbol{b}$ is vertical and the outermost shape corresponds to the critical stress at which the line cuts through the voids. The frames from left to right correspond to $\gamma_s = 0$, 0.5, 1.5 and 3.0 (see text) [68].

stress. An example of the line shape of an initially straight edge dislocation in copper bowing under increasing stress between two adjacent voids with $L = 316r_0$ and $D = 100r_0$, where r_0 is the dislocation core radius, is shown in Fig. 8. γ_s increases from left to right and is in units of $(Gb/4\pi)$ $\ln(R/r_0)$, where G is the shear modulus and R is the outer cut-off radius in the strain energy of a dislocation. (As usual in elasticity-based models of dislocations, r_0 enters as a unit of length, the value of which has to be chosen as seems appropriate). It can be seen that the dislocation bowout at the critical stress increases as γ_s increases and the line becomes almost tangential to the void at high γ_s, i.e. the line overcomes a void in an Orowan-like mode.

A summary of the critical stress a as a function of D, L and γ_s, for an isotropic medium is represented by Fig. 9. For comparison with results found in an earlier simulation of the Orowan process [70], σ, in units of Gb/L, is plotted against $\ln(\bar{D}/r_0)$, where $\bar{D}$ is the harmonic mean $(D^{-1} + L^{-1})^{-1}$.

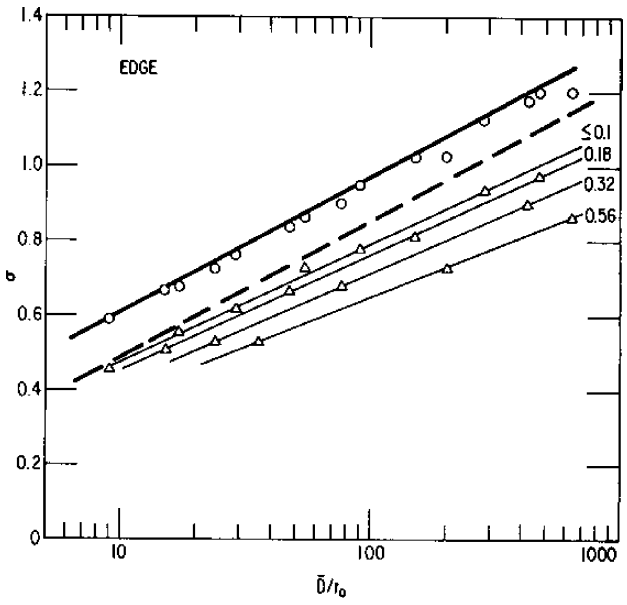

Fig. 9. Stress (units Gb/L) vs. $\bar{D}/r_0$, where $\bar{D}$ is the harmonic mean $(D^{-1} + L^{-1})^{-1}$, for an edge dislocation to pass a row of voids in an isotropic medium [68]. Triangles are for $\gamma_s = 0$ for the D/L ratios indicated. Circles are for $\gamma_s = 3$ (in units of $(Gb/4\pi)\ln(R/r_0)$) and the same D/L ratios. The dashed line is the Orowan stress for a row of impenetrable obstacles from [70].

This plot was found to give an excellent correlation for the Orowan stress for a row of impenetrable obstacles and is shown by the dashed line in the figure. Straight lines fit the void-passing stress values for a given D/L when $\gamma_s = 0$ and they have a lower gradient than that of the Orowan line, which is $1/2\pi$. When γ_s, increases, the stress for voids increases and the values fall on a single line when $\gamma_s = 3$. The gradient is $1/2\pi$ but the values are higher than the corresponding Orowan stress (this may result from dislocation termination/image effects in the void simulation).

Although more rigorous than a simple line tension approach, the modelling of [68,70] still suffers from the limitations of a continuum-based method, e.g. uncertainty over r_0 and an approximate treatment of the dislocation boundary condition near and at the void surface. These are overcome in a fully-atomistic simulation in recent modelling of the interaction of an $1/2\langle 1\,1\,1\rangle$ edge dislocation with voids in Fe (some preliminary results are in [2,3,61,62]). The model used [61] allows the dislocation to move over long distances under applied stress with prescribed strain rate at either zero or finite temperature. Crystallites containing up to 7.5 million atoms have been simulated. An example of information obtained for the interaction of a dislocation with a void of 339 vacancies (diameter ~2 nm) at 0 K is presented in Fig. 10. The dislocation was moved on a $\{1\,\bar{1}\,0\}$ glide plane under gradually increasing shear strain and the resulting dependence of stress, crystal energy and plastic displacement on strain is presented in the figure. The critical (maximum) stress is about 205 MPa (this equals 0.57 Gb/L, where $G = 62.5$ GPa, the value appropriate for a dislocation of the $1/2\langle 1\,1\,1\rangle$ $\{1\,\bar{1}\,0\}$ system in α-Fe [71]).

The critical stress has been obtained under static conditions for a range of void sizes and spacings. These stress values for $T = 0$ K are equivalent to the continuum model results obtained in [68,70] and are plotted in the same way for comparison in Fig. 11. The lines for the Orowan stress and void critical stress (for $\gamma_s = 3$) from Fig. 9 are included (the elastic core-cut-off paramenter r_0 has been taken simply as b for this comparison). It can be seen that the correlation between the critical stress and $\ln(\bar{D})$, which equals $\ln(D)$ when $D \ll L$, also applies to the results of atomic-level modelling. This agreement between two quite different sets of simulations is at first sight surprising, particularly since the model based on elasticity theory contains several approximations and it was not envisaged that it would apply

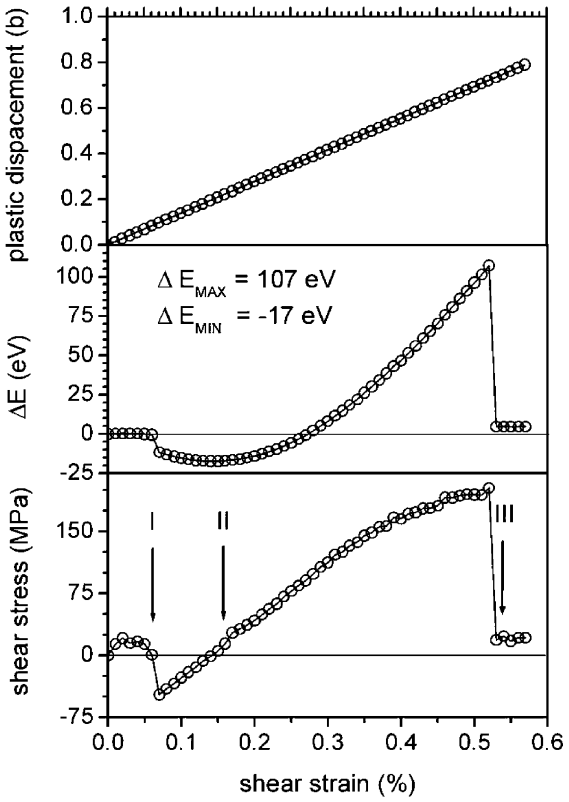

Fig. 10. Plastic displacement, excess of potential energy in the model crystallite and shear stress vs. strain during propagation of a 1/2⟨1 1 1⟩ edge dislocation through a row of 2 nm voids with spacing 41 nm in Fe [61]. Vertical arrows indicate: (I) the dislocation enters the voids; (II) it is pinned by the voids and bows between them; (III) it is released from the voids.

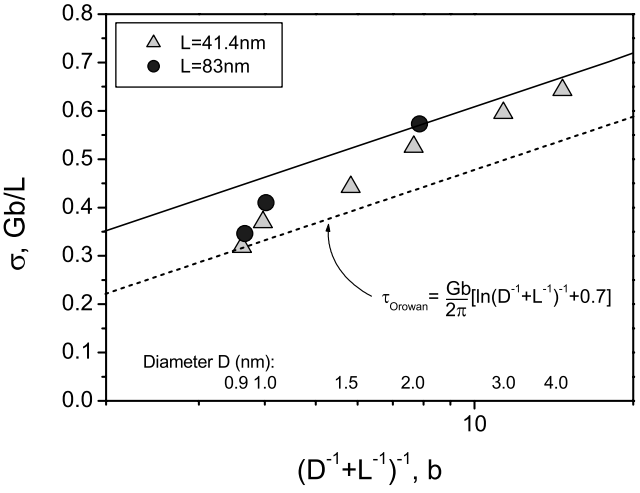

Fig. 11. Stress (units Gb/L) vs. $\bar{D}/b$ for an edge dislocation to pass a row of voids in an atomic model of Fe at $T = 0$ K. The D and L values are indicated. The dashed and full lines are those for the Orowan stress and for voids with $\gamma_s = 3$, respectively, taken from Fig. 9 for the continuum simulation of [68] with r_0 set equal to b.

to very small voids (the smallest D considered in [68] was $10r_0$, which is about 2.5 nm if $r_0 = b$). The reason for the agreement is that the dislocation segments that emerge from a void at the critical stress are almost parallel, which is the condition for the Orowan stress. They are screw in character, so in the critical configuration, the applied resolved shear stress acting over the length L draws out a screw dipole of spacing D, the 'line tension' of which is proportional to $\ln(D)$. The data in Fig. 11 for the smallest voids is seen not to fit this model quite so well, probably because the angle between the emergent segments in the critical condition is greater than zero [62].

In addition to the static modelling, MD simulations of a dislocation gliding under stress and meeting a row of voids have also been made over wide ranges of temperature and applied strain rate. Temperature and strain rate are important, even in regions free of obstacles. At non-zero temperature, a straight edge dislocation can move at shear stresses significantly below the Peierls stress, σ_p, which, for the iron model used, is ∼35 MPa [2,3,61]. The mechanism of motion can be described as thermal activation of kink nucleation and propagation with low activation energy (∼0.01 eV): the stress mainly affects the correlation in the motion of the kinks. At low stress ($<0.1\ \sigma_p$) this motion is similar to the random jumps of kinks, while at high stress ($\geq\sigma_p$) the motion of the whole dislocation line becomes uniform.

The dislocation–void interaction depends not only on void size and spacing, but also dislocation velocity, applied stress, strain rate and temperature. Some preliminary detail is in [62]. An interesting feature, which occurs even at $T = 0$ K, is that the interaction leads to climb of the dislocation as it leaves a void due to absorption of vacancies, i.e. the void shrinks, due to difficulty in creating a surface step on the emergent side of the void. The height of climb depends on the void size. To illustrate this effect, the evolution in the shape of a dislocation line due to repeated interaction with a 339-vacancy void at 100 K is presented in Fig. 12. Such a process could lead to the complete

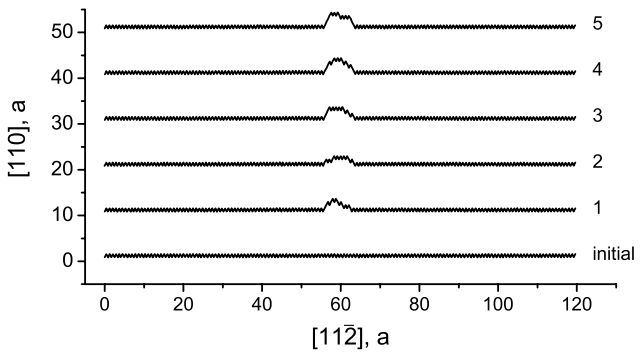

Fig. 12. Climb due vacancy absorption on a 1/2⟨1 1 1⟩ edge dislocation passing through a 2 nm (339-vacancy) void in Fe. The Burgers vector is perpendicular to the paper and the numbers on the left indicate the number of dislocation passes through the void. Results are for a crystallite of ∼2,200,000 atoms at 100 K.

absorption of a void after several dislocations have passed through it.

Similar modelling has also been performed for a model of the Fe–Cu alloy system [62]. This is relevant to pressure vessel steels, where small a concentration of Cu in solution forms coherent bcc precipitates under irradiation. For an $1/2\langle 1\,1\,1\rangle$ edge dislocation intersecting coherent Cu precipitates of diameter upto 6 nm, it is found that small precipitates in this size range are weaker obstacles than voids of the same size. This is because the critical breaking angle between the dislocation side arms at a precipitate is larger. However, the rate of increase of critical stress with precipitate size is larger than that for voids, and the strengths are similar (with zero breaking angle) when D is above about 4 nm. Furthermore, a dislocation-induced bcc $\Rightarrow$ fcc transformation of the copper precipitate occurs for precipitates above this size. This transformation effect was first observed in static modelling of screw dislocation–precipitate interaction [72,73], where is was estimated to produce a large strengthening effect, even for small precipitates. As with voids, climb due to dislocation–obstacle interaction is observed for precipitates and is strain-rate dependent—the higher the rate the more significant is the climb [62].

Large-scale atomic-level simulation of the effects of radiation-induced obstacles on dislocation motion under stress is still in its infancy. Clearly, there are many questions to be answered with regard to the multitude of interactions that can occur and the large variety of phenomena they give rise to. As noted above, linking the results to continuum-scale dislocation dynamics modelling is going to be crucial.

Acknowledgements

This research was supported by the Engineering and Physical Sciences Research Council.

References

[1] D.J. Bacon, F. Gao, Y.N. Osetsky, J. Nucl. Mater. 276 (2000) 1.
[2] D.J. Bacon, Y.N. Osetsky, Inter. Mater. Rev. 47 (2002).
[3] Y.N. Osetsky, D.J. Bacon, Nucl. Instrum. Methods B 202 (2003) 31.
[4] Y.N. Osetsky, D.J. Bacon, Nucl. Instrum. Methods B 180 (2001) 85.
[5] Y.N. Osetsky, D.J. Bacon, B.N. Singh, J. Nucl. Mater. 307–311 (2002) 866.
[6] F. Gao, D.J. Bacon, P.E.J. Flewitt, T.A. Lewis, J. Nucl. Mater. 249 (1997) 77.
[7] R.E. Stoller, J. Nucl. Mater. 276 (2000) 22.
[8] N. Soneda, S. Ishino, T. Diaz de la Rubia, Philos. Mag. Lett. 81 (2001) 649.
[9] K. Nordlund, L. Wei, Y. Zhong, R.S. Averback, Phys. Rev. B 57 (1998) R13965.
[10] K. Nordlund, R.S. Averback, J. Nucl. Mater. 276 (2000) 194.
[11] Y.N. Osetsky, D.J. Bacon, B.N. Singh, B. Wirth, J. Nucl. Mater. 307–311 (2002) 852.
[12] S.J. Wooding, L.M. Howe, F. Gao, A.F. Calder, D.J. Bacon, J. Nucl. Mater. 254 (1998) 191.
[13] F. Gao, D.J. Bacon, L.M. Howe, C.B. So, J. Nucl. Mater. 294 (2001) 288.
[14] C.S. Becquart, C. Domain, J.C. van Duysen, J.M. Raulot, J. Nucl. Mater. 294 (2001) 274.
[15] M. Spaczer, A. Caro, M. Victoria, T. Diaz de la Rubia, Phys. Rev. B 50 (1994) 13204.
[16] Y.N. Osetsky, D.J. Bacon, A. Serra, Philos. Mag. Lett. 79 (1999) 273.
[17] M. Ghaly, K. Nordlund, R.S. Averback, Philos. Mag. A 79 (1999) 795.
[18] N. de Diego, D.J. Bacon, Philos. Mag. A 80 (2000) 1393.
[19] M.J. Norgett, M.T. Robinson, I.M. Torrens, Nucl. Eng. Design 33 (1975) 50.
[20] D.J. Bacon, A.F. Calder, F. Gao, V.G. Kapinos, S.J. Wooding, Nucl. Instrum. Methods B 102 (1995) 37.
[21] M.L. Jenkins, J. Nucl. Mater. 216 (1994) 124.
[22] B.N. Singh, J.H. Evans, J. Nucl. Mater. 226 (1995) 277.
[23] M. Kiritani, J. Nucl. Mater. 276 (2000) 41.
[24] R.S. Averback, R. Benedek, K.L. Merkle, Phys. Rev. B 18 (1978) 4156.
[25] P. Jung, J. Nucl. Mater. 117 (1983) 70.
[26] J.H. Kinney, M.W. Guinan, Z.A. Munir, J. Nucl. Mater. 122 (1984) 1028.
[27] R.E. Stoller, J. Nucl. Mater. 276 (2000) 22.
[28] A. Alrnazouzi, M.J. Caturla, M. Alurralde, T. Diaz de la Rubia, M. Victoria, Nucl. Instrum. Methods B 153 (1999) 105.
[29] T. Diaz de la Rubia, A. Caro, M. Spaczer, Phys. Rev. B 47 (1993) 11483.
[30] M. Spaczer, A. Caro, M. Victoria, T. Diaz de la Rubia, Phys. Rev. B 50 (1994) 13204.
[31] F. Gao, D.J. Bacon, Philos. Mag. A 71 (1995) 43;
F. Gao, D.J. Bacon, Philos. Mag. A 71 (1995) 65.
[32] H. Zhu, R.S. Averback, M. Nastasi, Philos. Mag. A 71 (1995) 735.
[33] M. Spaczer, A. Almazouzi, R. Schaublin, M. Victoria, Rad. Eff. Def. Sol. 141 (1997) 349.
[34] C.A. English, M.L. Jenkins, Mater. Sci. Forum 15–18 (1987) 1003.
[35] M. Kiritani, J. Nucl. Mater. 216 (1994) 220.
[36] K. Nordlund, F. Gao, Appl. Phys. Lett. 74 (1999) 2720.
[37] V.G. Kapinos, Y.N. Osetsky, P.A. Platonov, J. Nucl. Mater. 184 (1991) 127.
[38] A.F. Calder, D.J. Bacon, J. Nucl. Mater. 207 (1993) 25.
[39] V.G. Kapinos, Y.N. Osetsky, P.A. Platonov, J. Nucl. Mater. 170 (1990) 66.
[40] A.J.E. Foreman, C.A. English, W.J. Phythian, Philos. Mag. A 66 (1992) 655.
[41] C.H. Woo, B.N. Singh, H. Heinisch, J. Nucl. Mater. 174 (1990) 190.
[42] R. Rauch, J. Peisl, A. Schmalzbauer, G. Wallner, J. Nucl. Mater. 168 (1989) 101.
[43] M.A. Kirk, M.L. Jenkins, H. Fukushima, J. Nucl. Mater. 276 (2000) 50.
[44] C.H. Woo, B.N. Singh, Philos. Mag. A 65 (1992) 889.
[45] F. Gao, D.J. Bacon, Y.N. Osetsky, P.E.J. Flewitt, T.A. Lewis, J. Nucl. Mater. 276 (2000) 213.
[46] Y.N. Osetsky, A.G. Mikhin, A. Serra, Philos. Mag. A 72 (1995) 361.
[47] M. Pelfort, Y.N. Osetsky, A. Serra, Philos. Mag. Lett. 81 (2001) 803.
[48] D.J. Bacon, F. Gao, Y.N. Osetsky, Nucl. Instrum. Methods Phys. Res., Sect. B 153 (1999) 87.
[49] D.J. Bacon, F. Gao, Y.N. Osetsky, J. Comput. Aided Mat. Des. 6 (2000) 225.
[50] Y.N. Osetsky, D.J. Bacon, A. Serra, B.N. Singh, S.I. Golubov, J. Nucl. Mater. 276 (2000) 65.
[51] N. de Diego, Y.N. Osetsky, D.J. Bacon, Metall. Trans. A 33 (2002) 783.
[52] N. Soneda, T. Diaz de Ia Rubia, Philos. Mag. A 81 (2001) 331.
[53] A.V. Barashev, Y.N. Osetsky, D.J. Bacon, Philos. Mag. A 80 (2000) 2709.
[54] S.I. Golubov, B.N. Singh, H. Trinkaus, J. Nucl. Mater. 276 (2000) 78.

[55] Y.N. Osetsky, D.J. Bacon, 2000 unpublished data.
[56] M.A. Puigvi, A. Serra, N. de Diego, Y.N. Osetsky, D.J. Bacon, Philos. Mag. A, in press.
[57] Y.N. Osetsky, A. Serra, V. Priego, J. Nucl. Mater. 276 (2000) 202.
[58] Y.N. Osetsky, D.J. Bacon, F. Gao, A. Serra, B.N. Singh, J. Nucl. Mater. 283–287 (2000) 784.
[59] B.N. Singh, J.H. Evans, A. Horsefield, P. Tofft, G.V. Muller, J. Nucl. Mater. 258–263 (1998) 865.
[60] M. Eldrup, B.N. Singh, S.J. Zinkle, T.S. Byun, K. Farrell, J. Nucl. Mater. (2003) in press.
[61] Y.N. Osetsky, D.J. Bacon, Modell. Simul. Mater. Sci. Eng. 11(2002) 427–446.
[62] Y.N. Osetsky, D.J. Bacon, Philos. Mag. A (2003) in press.
[63] D. Rodney, G. Martin, Phys. Rev. Lett. 82 (1999) 3272.
[64] D. Rodney, G. Martin, Phys. Rev. B 61 (2000) 8714.
[65] H. Trinkaus, B.N. Singh, A.J.E. Foreman, J. Nucl. Mater. 251 (1997) 172.
[66] T. Diaz de la Rubia, H. Zbib, T.A. Kraishi, B.D. Wirth, M. Victoria, M.J. Caturla, Nature 406 (2000) 871.
[67] K.C. Russell, L.M. Brown, Acta Metall. 20 (1972) 969.
[68] R.O. Scattergood, D.J. Bacon, Acta Metall. 30 (1982) 1665.
[69] J. Lothe, in: M.F. Ashby, et al. (Eds.), Nat. Bur. Standards, 1969, p. 317.
[70] R.O. Scattergood, D.J. Bacon, Philos. Mag. A 31 (1975) 179.
[71] D.J. Bacon, in: B.A. Bilby, K.J. Miller, J.R. Willis (Eds.), Cambridge University Press, Cambridge, 1985, p. 401.
[72] T. Harry, D.J. Bacon, Acta Mater. 50 (2002) 195.
[73] T. Harry, D.J. Bacon, Acta Mater. 50 (2002) 209.